Proper Orthogonal Decomposition and Dynamic Mode Decomposition of Delay-Differential Equations

B. Heizer, T. Kalmar-Nagy *

* *Department of Fluid Mechanics, Faculty of Mechanical Engineering, Budapest University of Technology and Economics, Budapest, Hungary (e-mail: kalmarnagy@ara.bme.hu)*

Abstract: Our work is based on the observation that delay-differential equations can be recast as partial differential equations of two variables. Thus the numerical solution of the delay equation can be thought of as a spatio-temporal process, and snapshot based methods like Proper Orthogonal Decomposition and Dynamic Mode Decomposition allow us to compute the eigenvalues of the evolution operator. The rightmost eigenvalues of the Hayes equation can be well approximated.

Keywords: Delay-differential equations, Proper Orthogonal Decomposition, Dynamic Mode Decomposition, Rightmost eigenvalues.

1. INTRODUCTION

Analysis of delay-differential equations is an ever-growing field. Our goal is to understand whether delay equations can be better understood or represented in terms of a natural "basis" (Asl and Ulsoy [2003], Amann et al. [2007], Michiels et al. [2011]). The general form of scalar delay-differential equations is

$$\frac{dx(t)}{dt} = f(x(t), x(t-\tau)), \tag{1}$$

$$x(t) = \theta(t), \quad -\tau \leq t \leq 0, \tag{2}$$

where $\theta(t)$ is the initial function. By introducing the so-called shift of time $u(t,s) = x(t+s)$, the initial value problem Eqs. (1, 2) can be recast into the following partial differential equation (Bellen and Maset [2000])

$$\frac{\partial u(t,s)}{\partial t} = \frac{\partial u(t,s)}{\partial s}, \quad s \in [-\tau, 0], \tag{3}$$

$$\left.\frac{\partial u(t,s)}{\partial t}\right|_{s=0} = f(u(t,0), u(t,-\tau)), \tag{4}$$

$$u(0,s) = \theta(s), \quad s \in [-\tau, 0]. \tag{5}$$

The $u(t,s)$ function can be viewed as a spatio-temporal representation of the initial value problem Eqs. (1, 2), where the variable s is the spatial dimension. The solution of Eqs. (1, 2) at time t_k is written into a column vector (called a snapshot)

$$\boldsymbol{x}_k = [u(t_k, s_1), u(t_k, s_2), ..., u(t_k, s_n)]^T. \tag{6}$$

A snapshot matrix $\boldsymbol{X}$ can be constructed from these snapshots

$$\boldsymbol{X} = \begin{bmatrix} | & | & & | \\ \boldsymbol{x}_1 & \boldsymbol{x}_2 & \dots & \boldsymbol{x}_m \\ | & | & & | \end{bmatrix}. \tag{7}$$

This representation of the problem allows us to apply snapshot based approaches like Proper Orthogonal Decomposition (Kutz [2013]) and Dynamic Mode Decomposition (Schmid [2010], Kutz et al. [2016], Tu et al. [2013]).

2. PROPER ORTHOGONAL DECOMPOSITION

Proper orthogonal decomposition (POD) is a powerful dimensionality reduction technique. The singular value decomposition

$$\boldsymbol{X} = \boldsymbol{U}\boldsymbol{\Sigma}\boldsymbol{V}^* \tag{8}$$

yields the matrix $\boldsymbol{U}$ that contains the orthogonal spatial modes (POD basis), $\boldsymbol{\Sigma}$ that contains the singular values σ_i, while all the temporal information is contained in matrix $\boldsymbol{V}$ and (* denotes the conjugate transpose). The singular values in $\boldsymbol{\Sigma}$ have an intuitive meaning, they are proportional with the energy content (L_1 norm of the singular values) of the corresponding modes in $\boldsymbol{U}$. With the orthogonal basis contained in $\boldsymbol{U}$, it is possible to obtain a reduced order model of the DDE through Galerkin projection. The solution $u(t,s)$ can be expanded in terms of n POD modes as

$$u(t,s) \approx \sum_{i=1}^{n} a_i(t)\phi_i(s), \tag{9}$$

where n is the number of POD modes and the ϕ_i's belong to the orthogonal set of POD modes. The corresponding $a_i(t)$'s can be determined by the Galerkin method. First, substituting Eq. (9) into Eq. (3) we get

$$\sum_{i=1}^{n} \phi_i(s)\frac{\partial a_i(t)}{\partial t} = \sum_{i=1}^{n} a_i(t)\frac{\partial \phi_i(s)}{\partial s}. \tag{10}$$

Projection of Eq. (10) onto the POD basis functions ϕ_j, $j = 1, ..., n$ yields

$$\frac{da_j(t)}{dt} = \frac{1}{\langle \phi_j(s), \phi_j(s) \rangle} \sum_{i=1}^{n} a_i(t) \left\langle \frac{\partial \phi_i(s)}{\partial s}, \phi_j(s) \right\rangle. \tag{11}$$

This set of ordinary differential equations can be written in matrix form

$$\frac{d\boldsymbol{a}}{dt} = \boldsymbol{L}\boldsymbol{a}, \tag{12}$$

where $\boldsymbol{a} = [a_1, a_2, ..., a_n]^T$ and the elements of $\boldsymbol{L}$ are given by

$$L_{ij} = \frac{\left\langle \frac{\partial \phi_i(s)}{\partial s}, \phi_j(s) \right\rangle}{\langle \phi_j(s), \phi_j(s) \rangle}. \tag{13}$$

The boundary conditions (4,5) enter into matrix $\boldsymbol{L}$ through relationship (8) between POD modes $\phi_i(s)$ and the snapshot matrix $\boldsymbol{X}$. The matrix $\boldsymbol{L}$ is a finite dimensional approximation of the infinitesimal generator of the DDE. By computing the spectra of $\boldsymbol{L}$ we can approximate the rightmost eigenvalues of the original system.

3. DYNAMIC MODE DECOMPOSITION

Dynamic mode decomposition (DMD) provides an alternative way to construct reduced order model of dynamic system from numerical data. Initially DMD was developed to decompose fluid flows and find spatio-temporal coherent structures (Schmid [2010]), however it became popular soon in a more general context (Brunton et al. [2016], Hua et al. [2016], Proctor and Eckhoff [2015]). DMD is based on the assumption that the snapshots $\boldsymbol{x}_k$ in the data matrix Eq. (7) are connected by a linear map

$$\boldsymbol{x}_{k+1} = \boldsymbol{A}\boldsymbol{x}_k. \tag{14}$$

In order to compute matrix $\boldsymbol{A}$ we construct the two matrices

$$\boldsymbol{X}_1 = \begin{bmatrix} | & | & & | \\ \boldsymbol{x}_1 & \boldsymbol{x}_2 & \dots & \boldsymbol{x}_{m-1} \\ | & | & & | \end{bmatrix}, \tag{15}$$

$$\boldsymbol{X}_2 = \begin{bmatrix} | & | & & | \\ \boldsymbol{x}_2 & \boldsymbol{x}_3 & \dots & \boldsymbol{x}_m \\ | & | & & | \end{bmatrix}. \tag{16}$$

from the data matrix $\boldsymbol{X}$ (see Eq. (7)). These matrices are connected by (assuming an underlying linear process)

$$\boldsymbol{X}_2 = \boldsymbol{A}\boldsymbol{X}_1. \tag{17}$$

The singular value decomposition of $\boldsymbol{X}_1$ is given by

$$\boldsymbol{X}_1 = \boldsymbol{U}_1 \boldsymbol{\Sigma}_1 \boldsymbol{V}_1^*. \tag{18}$$

Matrix $\boldsymbol{A}$ is computed as (+ denotes the Moore-Penrose pseudoinverse)

$$\boldsymbol{A} = \boldsymbol{X}_2 \boldsymbol{X}_1^+ = \boldsymbol{X}_2 \boldsymbol{V}_1 \boldsymbol{\Sigma}_1^{-1} \boldsymbol{U}_1^*. \tag{19}$$

If the underlying delay equation Eq. (1) is linear (i.e. $f(x(t), x(t-\tau)) = ax(t) + bx(t-\tau)$), then $\boldsymbol{A}$ is a finite dimensional approximation of its evolution operator. The eigenvalues of $\boldsymbol{A}$ approximate the spectrum of the evolution operator, which is related to the spectrum of Eq (1) by the exponential transform.

4. NUMERICAL RESULTS

We demonstrate the methods described in Sec. 2 and Sec. 3 on the Hayes equation (Hayes [1950]), which is one of the simplest delayed system in the following form

$$\frac{dx(t)}{dt} = ax(t) + bx(t-\tau). \tag{20}$$

The infinitely many eigenvalues of the Eq. (20) satisfy the characteristic equation:

$$\lambda - a - be^{-\lambda\tau} = 0. \tag{21}$$

We numerically solved the Eq. (20) with parameters $a = -3$, $b = -3.5$ and $\tau = 1$ for $t \in [0, 10]$ and initial function $\phi(t) = 1$. This numerical solution $x_{num}(t)$ was used to generate POD and DMD results.

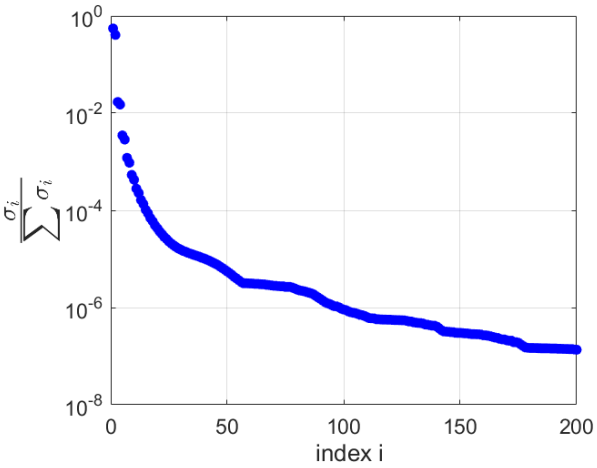

Fig. 1. The normalized singular values of $\boldsymbol{X}$

4.1 POD results

The energy content of the POD modes are depicted in Fig. (1). The first four POD modes contain 98.87% of the energy, these are illustrated in Fig. (2). We used these four modes for the expansion (9) and after projecting Eq. (20) onto these modes we get the following system of ordinary differential equations (the initial function is similarly projected, resulting in the initial conditions)

$$\frac{d}{dt}\begin{bmatrix} a_1 \\ a_2 \\ a_3 \\ a_4 \end{bmatrix} = \begin{bmatrix} -0.05 & 1.84 & 0.01 & -0.01 \\ -3.24 & -0.11 & -0.02 & -0.02 \\ -0.59 & -3.24 & -1.09 & 6.06 \\ -1.75 & -1.06 & -10.51 & -1.17 \end{bmatrix} \begin{bmatrix} a_1 \\ a_2 \\ a_3 \\ a_4 \end{bmatrix}. \tag{22}$$

The solutions of Eq. (22) are shown Fig. (3). Eigenvalues of the coefficient matrix in Eq. (22) are approximating the eigenvalues of the evolution operator of Eq. (20). In Fig. (5) we compared these 4 approximate eigenvalues (2 complex pairs) with those obtained from the Matlab package published by Breda et al. [2014] (a homotopy-based method to find the spectrum of delay equations is described in Surya et al. [2017]). By increasing the number of POD modes gives a more accurate approximation for the rightmost eigenvalues. Near the eigenvalues the magnitude of the characteristic function (21) is small. Thus substituting the computed eigenvalues into (21) should result in a residual of small magnitude. This is shown in Fig. (6) for increasing number of POD modes.

4.2 DMD results

When the pseudo-inverse $\boldsymbol{X}_1^+$ calculated, a rank reduced $\boldsymbol{A}$ (denoted by $\tilde{\boldsymbol{A}}$) can be computed by truncating the matrices $\boldsymbol{U}_1$, $\boldsymbol{V}_1$ and $\boldsymbol{\Sigma}_1$. For example, a rank-4 approximation of $\boldsymbol{A}$ is given by

$$\tilde{\boldsymbol{A}} = \begin{bmatrix} 0.9971 & -0.0800 & -0.0215 & 0.0371 \\ 0.0464 & 0.9950 & -0.0850 & 0.0057 \\ 0.0004 & -0.0008 & 0.9324 & 0.2509 \\ -0.0003 & 0.0005 & -0.1454 & 0.9660 \end{bmatrix}. \tag{23}$$

The computation of the DMD modes ψ_i (which come in conjugate transpose pairs) is described in Section 1.4 of

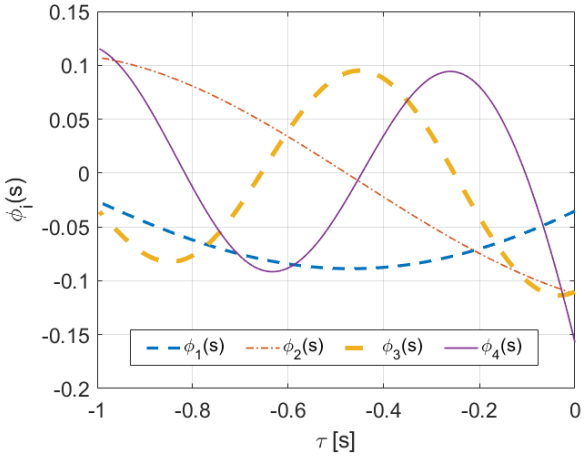

Fig. 2. The first four POD modes

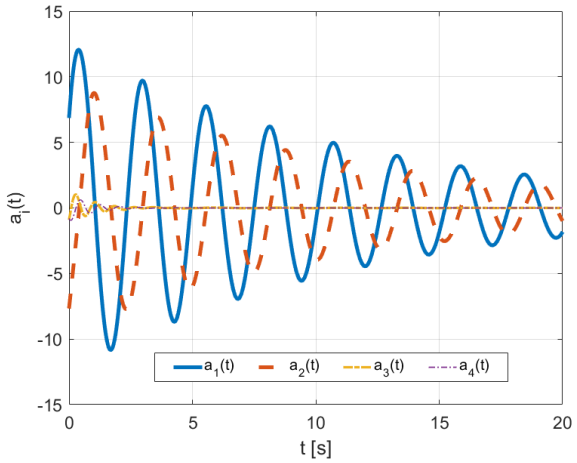

Fig. 3. The $a_i(t)$ functions corresponding to the first 4 POD modes

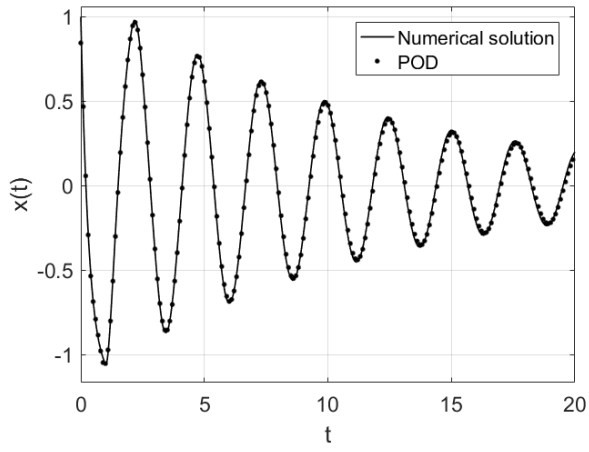

Fig. 4. Numerical solution and POD approximation

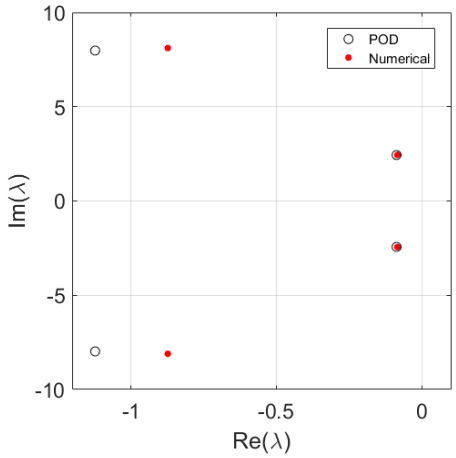

Fig. 5. Comparison of the computed eigenvalues

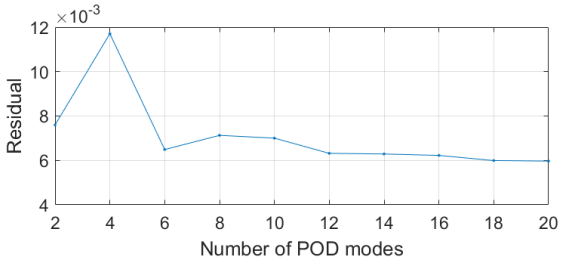

Fig. 6. Residual at the approximated rightmost eigenvalue

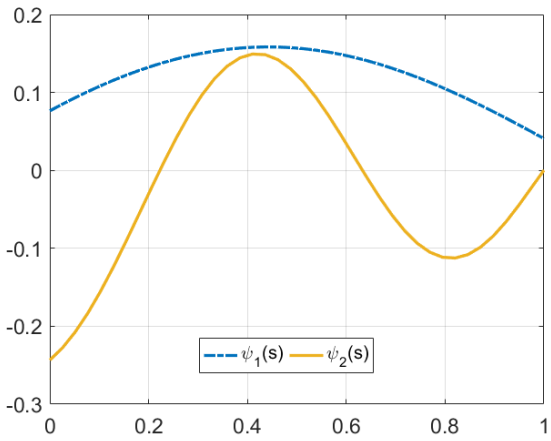

Fig. 7. Real part of the first two DMD mode pairs

Kutz et al. [2016]. The real part of the first two DMD mode pairs and the real part of their amplitudes are shown in Figs. (7) and (8), respectively. The numerical solution $x_{num}(t)$ and its approximation computed by DMD are shown in Fig. (9). Eigenvalues of $\tilde{\boldsymbol{A}}$ are approximating the eigenvalues of Eq. (20) (Fig. (10)). By increasing the rank of $\tilde{\boldsymbol{A}}$, the DMD gives better approximation for the rightmost eigenvalues. Near the eigenvalues the magnitude of the characteristic function (21) is small. Thus substituting the computed eigenvalues into (21) should result in a residual of small magnitude. This is shown in Fig. (11) for increasing number of POD modes.

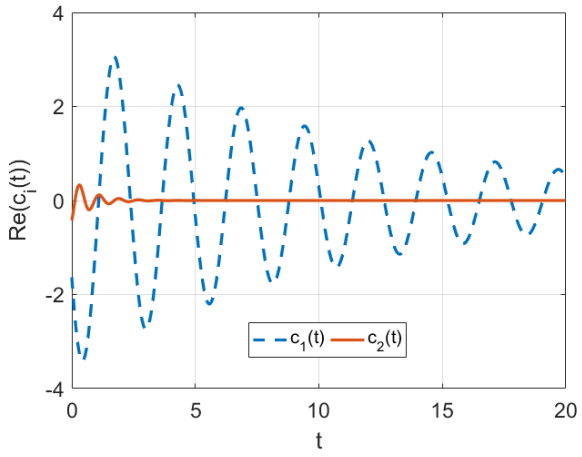

Fig. 8. The amplitudes of the first two DMD mode pairs

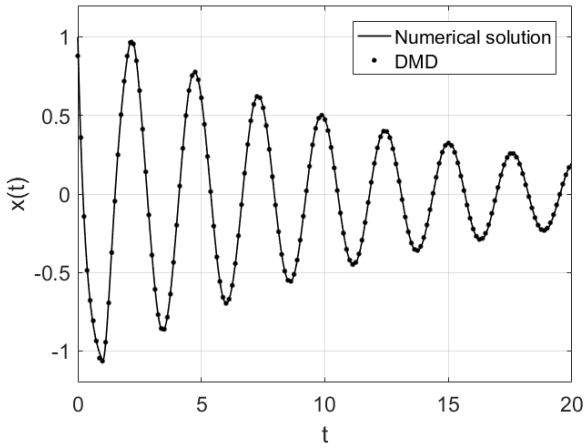

Fig. 9. Numerical solution and DMD approximation

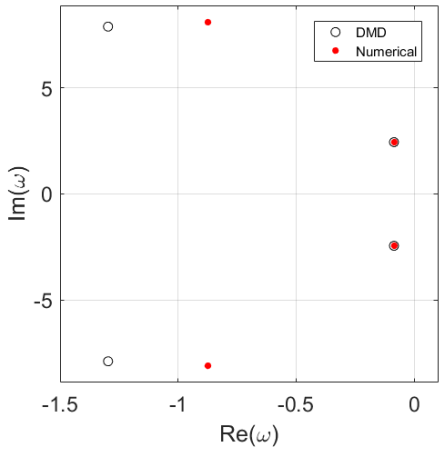

Fig. 10. Comparison of the computed eigenvalues

5. DISCUSSION AND CONCLUSION

Two data-driven methods were presented to compute the eigenvalues (and rightmost eigenvalues in particular) of delay-differential equation based on snapshots of the numerical solution $x_{num}(t)$. This was shown by solving the Hayes equation for a parameter pair (a, b), but numerical

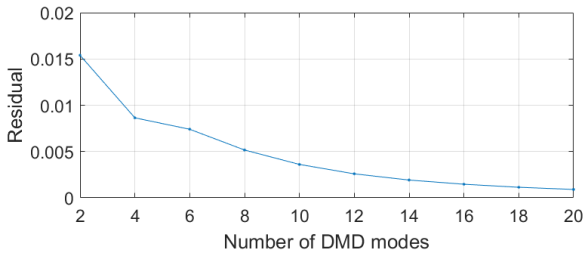

Fig. 11. Residual at the approximated rightmost eigenvalue

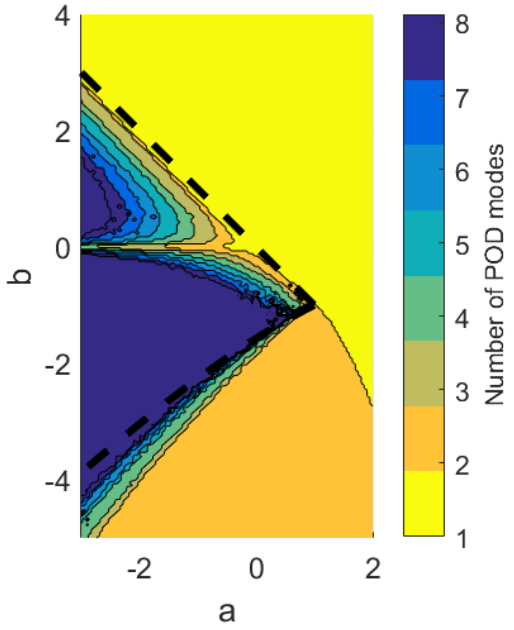

Fig. 12. The stability chart of the Hayes equation, colored by the number of POD modes used to reconstruct the original data less than 0.1% error. The thick dashed line is the stability boundary.

experiments show that our findings apply well for other parameter pairs. Further investigations in the range of applicability and error estimation will be the topic of a full research paper.

There is an interesting connection between the energy content of the POD modes and the stability of the Hayes equation. We found that in the stable region more POD modes were needed to reach a certain energy content. We attribute this to the fact that in the unstable region the most unstable modes overwhelm the others. The region where already one mode captured the behavior of the system, we found a single positive real leading eigenvalue, while where the dynamics was approximated by two modes, the leading eigenvalues were a complex conjugate pair. In Fig. (12) we depict how many POD modes needed to reconstruct to 99.99% of the energy content for a given (a, b) parameter pair.

REFERENCES

Amann, A., Schöll, E., and Just, W. (2007). Some basic remarks on eigenmode expansions of time-delay dynamics. *Physica A: Statistical Mechanics and its Applications*, 373, 191–202.

Asl, F.M. and Ulsoy, A.G. (2003). Analysis of a system of linear delay differential equations. *Journal of Dynamic Systems, Measurement, and Control*, 125(2), 215–223.

Bellen, A. and Maset, S. (2000). Numerical solution of constant coefficient linear delay differential equations as abstract cauchy problems. *Numerische Mathematik*, 84(3), 351–374.

Breda, D., Maset, S., and Vermiglio, R. (2014). *Stability of Linear Delay Differential Equations: A Numerical Approach with MATLAB*. Springer.

Brunton, B.W., Johnson, L.A., Ojemann, J.G., and Kutz, J.N. (2016). Extracting spatial–temporal coherent patterns in large-scale neural recordings using dynamic mode decomposition. *Journal of neuroscience methods*, 258, 1–15.

Hayes, N. (1950). Roots of the transcendental equation associated with a certain difference-differential equation. *Journal of the London Mathematical Society*, 1(3), 226–232.

Hua, J.C., Roy, S., McCauley, J.L., and Gunaratne, G.H. (2016). Using dynamic mode decomposition to extract cyclic behavior in the stock market. *Physica a: Statistical mechanics and its applications*, 448, 172–180.

Kutz, J.N. (2013). *Data-driven modeling & scientific computation: methods for complex systems & big data*. Oxford University Press.

Kutz, J.N., Brunton, S.L., Brunton, B.W., and Proctor, J.L. (2016). *Dynamic mode decomposition: data-driven modeling of complex systems*, volume 149. SIAM.

Michiels, W., Jarlebring, E., and Meerbergen, K. (2011). Krylov-based model order reduction of time-delay systems. *SIAM Journal on Matrix Analysis and Applications*, 32(4), 1399–1421.

Proctor, J.L. and Eckhoff, P.A. (2015). Discovering dynamic patterns from infectious disease data using dynamic mode decomposition. *International health*, 7(2), 139–145.

Schmid, P.J. (2010). Dynamic mode decomposition of numerical and experimental data. *Journal of fluid mechanics*, 656, 5–28.

Surya, S., Vyasarayani, C., and Kalmár-Nagy, T. (2017). Homotopy continuation for characteristic roots of delay differential equations using the lambert w function. *Journal of Vibration and Control*, DOI: 10.1077546317717629.

Tu, J.H., Rowley, C.W., Luchtenburg, D.M., Brunton, S.L., and Kutz, J.N. (2013). On dynamic mode decomposition: theory and applications. *arXiv preprint arXiv:1312.0041*.